Photoinduced Energy and Electron Transfer Reactions in Lamellar Polyanion/Polycation Thin Films: Toward an Inorganic "Leaf"

David M. Kaschak, John T. Lean, Chad C. Waraksa, Geoffrey B. Saupe, Hisanao Usami, and Thomas E. Mallouk*

Contribution from the Department of Chemistry, The Pennsylvania State University, University Park, Pennsylvania 16802

Received August 19, 1998

Abstract: Sequential adsorption of polyanions and polycations was used to make a five-component energy/electron-transfer cascade, which mimics some of the functions of natural photosynthetic assemblies. The photon antenna part of the system consists of coumarin- and fluorescein-derivatized poly(allylamine hydrochloride) (Coum-PAH and Fl-PAH), palladium(II)tetrakis(4-*N,N,N*-trimethylanilinium) porphyrin (PdTAPP^{4+}) or palladium(II)tetrakis(4-sulfonatophenyl) porphyrin (PdTSPP^{4-}) layers, interleaved with anionic Zr(HPO$_4$)$_2$· H$_2$O (α-ZrP) sheets. α-ZrP or HTiNbO$_5$ sheets separate the porphyrin electron donor from a polyviologen electron acceptor layer. Layer-by-layer growth of these thin film assemblies was characterized by atomic force microscopy (AFM) and ellipsometry on planar supports, and by elemental analysis, surface area measurements, and transmission electron microscopy high on surface area silica supports. UV−vis absorption and steady-state emission spectroscopies showed that the overall energy/electron-transfer reaction (Coum → Fl → PdTSPP^{4-} → viologen) occurs with approximate quantum yields of 0.47 and 0.61 for systems containing α-ZrP and HTiNbO$_5$ sheets, respectively. Transient diffuse reflectance spectroscopy established that a porphyrin−viologen charge separated state is formed in the reaction, and that it has an exceptionally long-lived component ($\tau \approx$ 900 μs) with the HTiNbO$_5$ spacer. It is inferrred that the semiconducting HTiNbO$_5$ sheets play an active role in relaying the electron from photoexcited PdTSPP^{4-} to the viologen electron acceptor.

Introduction

Natural photosynthesis involves a series of intermolecular energy and electron transfer reactions that convert light to chemical energy. The first steps in this process occur in light harvesting complexes (LHCs) that contain axially symmetric bundles of chromophore pairs. Excitation is funneled down the axis of the LHC by a series of ultrafast energy transfer reactions. The energy passes through progressively redder regions, and finally reaches a reaction center in which a series of unidirectional electron-transfer reactions occurs. One of the most striking aspects of these assemblies, which has been revealed by crystallographic studies,[1] is the exquisite level of control that nature exerts over intermolecular distances, orientations, and local environments. The juxtaposition of chromophores tunes their electronic interactions, which govern both their absorptive/ emissive properties and the kinetics of energy transfer. The rates of intermolecular electron transfer reactions are similarly regulated in order to ensure that the vectorial, or forward, pathway is the kinetically dominant one.

The goals of artificial photosynthesis are to mimic different aspects of the natural process, and ultimately to produce efficient photoconversion systems or devices. One of the biggest stumbling blocks in this work has been to provide a framework for organizing molecules in space, at the level of complexity and control needed for high conversion efficiency. Two basic approaches to this problem have emerged. One is to make supermolecules, in which the order and spacing of subunits in a chain is fixed by covalent bonds.[2] Although this method is

quite effective for model studies, the synthesis becomes increasingly demanding as more chromophores and redox-active units are added. Another strategy is to use supramolecular supports or self-assembling systems (such as polymers,[3] dendrimers,[4] sol−gel glasses,[5] micelles,[6] vesicles,[7] particle aggregates,[8] and zeolites[9]). In this case the synthesis is easier, but it is hard to attain the required level of complexity. A combined approach, in which relatively small supermolecules (dyads or triads) are organized into a larger self-assembling system, is also possible.

(1) (a) Huber, R. *Angew. Chem., Int. Ed. Engl.* **1989**, *28*, 848. (b) Sauer, K.; Scheer, H.; Sauer, P. *Photochem. Photobiol.* **1987**, *46*, 427.

(2) (a) Gust, D.; Moore, T. A.; Moore, A. L. *Acc. Chem. Res.* **1993**, *26*, 198. (b) Gust, D.; Moore, T. A.; Moore, A. L.; Lee, S.-J.; Bittersman, E.; Juttrull, D. K.; Rehms, A. A.; DeGraziano, J. M.; Ma, X. C.; Gao, F.; Belford, R. E.; Trier, T. T. *Science* **1990**, *248*, 199. (c) Gust, D.; Moore, T. A.; Moore, A. L.; MacPherson, A. N.; Lopez, A.; DeGraziano, J. M.; Gouni, I.; Bittersman, E.; Seely, G. R.; Gao, F.; Nieman, R. A.; Ma, X. C.; Demanche, L.; Hung, S.-C.; Luttrull, D. K.; Lee, S.-J.; Kerrigan, P. K. *J. Am. Chem. Soc.* **1993**, *115*, 11141. (d) Wasielewski, M. R. *Chem. Rev.* **1992**, *92*, 435.

(3) (a) Sassoon, R. E.; Gershuni, S.; Rabani, J. *J. Phys. Chem.* **1992**, *96*, 4692. (b) Rabani, J. in *Photoinduced Electron Transfer*; Fox, M. A., Chanon, M., Eds.; Elsevier: Amsterdam, 1988, Part B, pp 642−696. (c) Sassoon, R. E. *J. Am. Chem. Soc.* **1985**, *107*, 6133. (d) Rabani, J.; Sassoon, R. E. *J. Photochem.* **1985**, *29*, 7. (e) Whitesell, J. K.; Chang, H. K.; Fox, M. A.; Galoppni, E.; Watkins, D. M.; Fox, H.; Hong, B. *Pure Appl. Chem.* **1996**, *68*, 1469. (f) Watkins, D. M.; Fox, M. A. *J. Am. Chem. Soc.* **1996**, *118*, 4344. (g) Fossum, R. D.; Fox, M. A. *J. Am. Chem. Soc.* **1997**, *119*, 1197. (h) Dupray, L. N.; Devenney, M.; Striplin, D. R.; Meyer, T. J. *J. Am. Chem. Soc.* **1997**, *119*, 10243. (i) Slate, C. A.; Striplin, D. R.; Moss, J. A.; Chen, P.; Erickson, B. W.; Meyer, T. J. *J. Am. Chem. Soc.* **1998**, *120*, 4885.

(4) (a) Balzani, V.; Campagna, S.; Denti, G.; Juris, A.; Serroni, S.; Venturi, M. *Acc. Chem. Res.* **1998**, *31*, 26. (b) Serroni, S.; Juris, A.; Venturi, M.; Campagna, S.; Resino, I. R.; Denti, G.; Credi, A.; Balzani, V. *J. Mater. Chem.* **1997**, *7*, 1227. (c) Issberner, J.; Voegtle, F.; De Cola, L.; Balzani, V. *Chem. Eur. J.* **1997**, *3*, 706. (d) Archut, A.; Vogtle, F.; De Cola, L.; Azzellini, G. C.; Balzani, V. *Chem. Eur. J.* **1998**, *4*, 699. (e) Serroni, S.; Campagna, S.; Denti, G.; Juris, A.; Venture, M.; Balzani, V. *Adv. Dendritic Macromol.* **1996**, *3*, 61. (f) Stewart, G. M.; Fox, M. A. J. *Am. Chem. Soc.* **1996**, *118*, 4354.

For example, electron donor–acceptor dyads immobilized on zeolites act as a building block of more efficient self-assembling triads.[10] Recently, a vesicle/supermolecule combination was used to make a photochemical proton pump, and to drive the phosphorylation of adenosine diphosphate (ADP) with visible light.[11]

Self-assembled multilayer films provide, in principle, a synthetically simple way to access complex supramolecular structures. The idea is to grow monolayers of photo- and redox-active molecules on top of each other in the appropriate sequence. Early studies in this area used Langmuir–Blodgett (L–B) films,[12] and more recent studies focused on covalently linked molecular layers.[13] This approach has serious limitations for real devices. L–B films are tricky to prepare, easy to disrupt, and not useful with the high surface area supports needed to achieve adequate light absorption. Covalent systems, such as metal phosphonates, allow a relatively small cross sectional area per headgroup.[14] Multilayer structures of this type that incorporate larger chromophores become poorly ordered after a few layers.

An attractive alternative to covalent multilayer deposition is polyelectrolyte self-assembly, which is easy to implement and forgiving with respect to molecular size.[15] Recently, we reported light-driven electron and energy transfer reactions in lamellar dyads of organic polycations separated by anionic α-zirconium phosphate (α-ZrP) sheets.[16,17] In these "club sandwich" structures, the nanometer-thick inorganic sheets prevent the interpenetration of redox-active layers, and thereby inhibit back electron-transfer reactions. In this paper, we describe the construction of more complex systems, which perform sequential energy and electron-transfer reactions. By using three complementary chromophores, excitation is collected from a substantial fraction of the visible spectrum and funneled to a trap molecule that forms a long-lived triplet excited state. This trap molecule then transfers an electron to an acceptor in the next layer. In these four-component systems, the α-ZrP sheets act as passive spacers, and the back electron-transfer reaction is relatively fast. The charge separation quantum efficiency and lifetime can be significantly increased by introducing an active spacer, which is an oxide semiconductor sheet. In this case, one has a five-component energy/electron-transfer cascade in which there are no covalent bonds between any of the photo- or redox-active components.

Experimental Section

1. Materials. Poly(4-vinyltoluene) (PVT) 80 000 MW, 4,4′-dipyridyl, fluorescein-5-isothiocyanate, *N*-bromosuccinimide, and poly(allylamine hydrochloride) (PAH), 50 000 MW, were used as received from Aldrich. 7-diethylaminocoumarin-3-carboxylic acid succinimidyl ester was purchased from Molecular Probes, Inc. and used immediately as received. Palladium(II)tetrakis(4-*N*,*N*,*N*-trimethylanilinium) porphyrin, chloride salt ($PdTAPP^{4+}$), and palladium(II)tetrakis(4-sulfonatophenyl) porphyrin, sodium salt ($PdTSPP^{4-}$) were used as received from Midcentury Chemicals. Microcrystalline α-Zr(HPO_4)$_2$·H_2O (α-ZrP) [18] and $HTiNbO_5$ [19] were available from earlier studies.

2. Synthesis and Characterization of Fluorescein, Coumarin, and Viologen Polycations. (a) Fluorescein-PAH Polymer (Fl-PAH). PAH (0.1 g, 1×10^{-3} equiv) was dissolved in 5 mL water with 0.045 g $NaHCO_3$ (0.5×10^{-3} moles). To this solution was added 100 mg fluorescein-5-isothiocyanate (2.57×10^{-4} moles) in 15 mL of dimethylformamide (DMF). The flask was swirled occasionally while kept in the dark at room temperature for 3 h. The solution was acidified with 0.5 mL 5% HCl, and the polymer was then immediately precipitated with excess acetone. The polymer was redissolved and reprecipitated twice using water (5 mL) and acetone, respectively. The yellow-orange polymer was then dried in air and stored in the dark.

^{1}H NMR of Fl-PAH showed three broad resonances at 1.35, 1.9, and 2.92 ppm, which were assigned to CH_2 and CH groups in the polymer chain. UV–vis absorption spectra showed the characteristic broad absorbance band of fluorescein at 500 nm, and steady-state fluorescence spectra also showed the corresponding emission band with a maximum at 530 nm. The loading of Fl groups in the Fl-PAH polymer was calculated from UV–vis spectra to be 1 per 50 monomer units, using the literature extinction coefficient of Fl (76 900 $M^{-1}cm^{-1}$).[20]

(b) Coumarin-PAH Polymer (Coum-PAH). PAH (0.1 g, 1×10^{-3} equiv) was dissolved in 5 mL water with 0.045 g $NaHCO_3$ (5.0 ×

(5) (a) Fan, J.; Gafney, H. D *J. Phys. Chem.* **1994**, *98*, 13058. (b) Braun, M.; Gafney, H. D. *J. Phys. Chem.* **1994**, *98*, 8108. (c) Fan, J.; Tysoe, S.; Strekas, T. C.; Gafney, H. D.; Serpone, N.; Lawless, D. *J. Am. Chem. Soc.* **1994**, *116*, 5343. (d) Slama-Schwok, A.; Avnir, D.; Ottolenghi, M. *J. Phys. Chem.* **1989**, *93*, 7544. (e) Slama-Schwok, A.; Avnir, D.; Ottolenghi, M. *J. Am. Chem. Soc.* **1991**, *113*, 3984. (f) Slama-Schwok, A.; Avnir, D.; Ottolenghi, M. *Nature* **1992**, *355*, 240.

(6) (a) Brugger, P.-A.; Grätzel, M. *J. Am. Chem. Soc.* **1980**, *102*, 2461. (b) Kang, Y. S.; McManus, H. J. D.; Liang, K.; Kevan, L. *J. Phys. Chem.* **1994**, *98*, 1044.

(7) (a) Humphry-Baker, R.; Thompson, D. H.; Lei, Y.; Hope, M. J.; Hurst, J. K. *Langmuir* **1991**, *7*, 2592. (b) Patterson, B. C.; Thompson, D. H.; Hurst, J. K. *J. Am. Chem. Soc.* **1988**, *110*, 3656. (c) Hurst, J. K.; Thompson, D. H. P.; Connolly, J. S. *J. Am. Chem. Soc.* **1987**, *109*, 507.

(8) (a) Kamat, P. V. *Chem. Rev.* **1993**, *93*, 267. (b) Kamat, P. V. in *Kinetics and Catalysis in Microheterogeneous Media*; Grätzel, M., Kalyanasundaram, K., Eds.; Marcel Dekker: New York, 1991; pp 376–436. (b) Ahmadi, T. S.; Wang, Z. L.; Green, T. C.; Henglein, A.; El-Sayed, M. A. *Science* **1996**, *272*, 1924. (c) Korgel, B. A.; Fitzmaurice, D. *Adv. Mater.* **1998**, *10*, 661. (d) Fitzmaurice, D.; Frei, H.; Rabani, J. *J. Phys. Chem.* **1995**, *99*, 9176.

(9) (a) Faulkner, L. R.; Suib, S. L.; Renschler, C. L.; Green, J. M.; Bross, P. R. In *Chemistry in Energy Production*; Wymer, R. G., Keller, O. L., Eds.; John Wiley and Sons: New York, 1982; pp 99–114. (b) Dutta, P. K.; Incavo, J. A. *J. Phys. Chem.* **1987**, *91*, 4443. (c) Incavo, J. A.; Dutta, P. K. *J. Phys. Chem.* **1990**, *94*, 3075. (d) Dutta, P. K.; Turbeville, W. *J. Phys. Chem.* **1992**, *96*, 5024. (e) Dutta, P. K.; Turbeville, W. *J. Phys. Chem.* **1992**, *96*, 9410. (f) Sankaraman, S.; Yoon, K. B.; Yake, T.; Kochi, J. *J. Am. Chem. Soc.* **1991**, *113*, 1419. (g) Liu, X.; Liu, K.-K.; Thomas, J. K. *J. Phys. Chem.* **1989**, *93*, (3), 4120. (h) Borja, M.; Dutta, P. K. *Nature* **1993**, *362*, 43. (i) Maruszewski, K.; Strommen, D. P.; Kincaid, J. R. *J. Am. Chem. Soc.* **1993**, *115*, 8345. (j) Ledney, M.; Dutta, P. K. *J. Am. Chem. Soc.* **1995**, *117*, 7687. (k) Kim, Y. I.; Mallouk, T. E. *J. Phys. Chem.* **1992**, *96*, 2879.

(10) (a) Krueger, J. S.; Mayer, J. E.; Mallouk, T. E. *J. Am. Chem. Soc.* **1988**, *110*, 8232. (b) Yonemoto, E. H.; Kim, Y. I.; Schmehl, R. H.; Wallin, J. O.; Shoulders, B. A.; Richardson, B. R.; Haw, J. F.; Mallouk, T. E., *J. Am. Chem. Soc.* **1994**, *116*, 10557. (c) Sykora, M.; Maruszewski, K.; Treffert-Ziemelis, S. M.; Kincaid, J. R. *J. Am. Chem. Soc.* **1998**, *120*, 3490.

(11) (a) Steinberg-Yfrach, G.; Rigaud, J.-L.; Durantini, E. N.; Moore, A. L.; Gust, D.; Moore, T. A. *Nature* **1998**, *392*, 479. (b) Steinberg-Yfrach, G.; Liddell, P. A.; Hung, S.-C.; Moore, A. L.; Gust, D.; Moore, T. A. *Nature* **1997**, *385*, 239.

(12) (a) Kuhn, H. *J. Chem. Phys.* **1970**, *53*, 101. (b) Fromherz, P.; Reinbold, G. *Thin Solid Films* **1988**, *160*, 347. (c) Fromherz, P.; Arden, W. *Ber. Bunsen-Ges. Phys. Chem.* **1980**, *84*, 2045. (d) Fujihira, M. In *Photochemical Processes in Organized Molecular Systems*; K. Honda, Ed.; North-Holland: Amsterdam, 1991; pp 463–482. (e) Yamamoto, M.; et al. In *Photochemical Processes in Organized Molecular Systems*; Honda, K., Ed.; North-Holland: Amsterdam, 1991; pp 329–341. (f) Ahuja, R. C.; Mobius, D.; Matsumoto, M. *Thin Solid Films* **1992**, *210*, 60.

(13) (a) Byrd, H.; Suponeva, E. P.; Bocarsly, A. B.; Thompson, M. E. *Nature* **1996**, *380*, 610. (b) Vermeulen, L. A.; Thompson, M. E. *Nature* **1992**, *358*, 656. (c) Ungashe, S. B.; Wilson, W. L.; Katz, H. E.; Scheller, G. R.; Putvinski, T. M. *J. Am. Chem. Soc.* **1992**, *114*, 8717. (d) Vermeulen, L. A.; Snover, J. L.; Sapochak, L. S.; Thompson, M. E. *J. Am. Chem. Soc.* **1993**, *115*, 11767. (e) Snover, J. L.; Thompson, M. E. *J. Am. Chem. Soc.* **1994**, *116*, 765.

(14) (a) Cao, G.; Hong, H.-G.; Mallouk, T. E. *Acc. Chem. Res.* **1992**, *25*, 420. (b) Mallouk, T. E.; Kim, H.-N.; Ollivier, P. J.; Keller, S. W. in *Comprehensive Supramolecular Chemistry*; Alberti, G., Bein, T., Eds.; Elsevier: Oxford, UK, 1996; Vol. 7, pp 189–217.

(15) Decher, G. *Science* **1997**, *277*, 1232.

(16) Keller, S. W.; Johnson, S. A.; Brigham, E. S.; Yonemoto, E. H.; Mallouk, T. E. *J. Am. Chem. Soc.* **1995**, *117*, 12879.

(17) Kaschak, D. M.; Mallouk, T. E. *J. Am. Chem. Soc.* **1996**, *118*, 4222.

(18) Keller, S. W.; Kim, H.-N.; Mallouk, T. E. *J. Am. Chem. Soc.* **1994**, *116*, 8817.

(19) Saupe, G. B.; Kim, W.; Schmehl, R. H.; Mallouk, T. E. *J. Phys. Chem. B* **1997**, *101*, 2491.

(20) Sjöback, R.; Nygren, J.; Kubista, M. *Spectrochim. Acta, Part A* **1995**, *A51*, L7.

10^{-4} mol). To this solution was added 100 mg 7-diethylaminocoumarin-3-carboxylic acid succinimidyl ester (2.79×10^{-4} mol) in 15 mL DMF. The reaction conditions and workup were the same as described above for Fl-PAH. The yellow coumarin-derivatized polymer was then dried in air and stored in the dark. ^{1}H NMR again showed only broad resonances attributed to the CH and CH_2 groups of the PAH polymer. UV–vis absorption spectra showed a coumarin band at 412 nm, from which a dye loading of 1 Coum/40 PAH was calculated, and fluorescence spectra showed the corresponding emission peak at 485 nm.

(c) Brominated PVT (PVTBr). Polyvinyltoluene (Aldrich, 5.0 g, M_w 80 000) was dissolved in CCl_4 (100 mL). One equiv N-bromosuccinimide (Aldrich, 7.5 g, 42 mmol) for each repeating unit of the polymer and a catalytic amount of azobis(isobutyronitrile) (AIBN) (Aldrich, 0.2 g, 1 mmol) were added to the solution. The mixture was refluxed under a 300 W Sylvania flood lamp for 2 h, allowed to cool, and then filtered. The solvent was removed under reduced pressure to give a yellow precipitate, which was redissolved in $CHCl_3$ and washed twice with water. The organic layer was dried over anhydrous Na_2SO_4 and filtered. The solvent was removed under reduced pressure to yield PVTBr (8.4 g) in which about 56% of the methyl groups were brominated (estimated from ^{1}H NMR integration): ^{1}H NMR ($CDCl_3$) 1.2–1.8 (br, 3H, CH and CH_2), 2.0–2.4 (br, 1.3H, CH_3), 4.1–4.5 (br, 1.3H, CH_2Br), 6.1–7.2 (d br, 4H, C_6H_4). GPC analysis using polystyrene standards gave M_w 9.1×10^4, M_n 5.8×10^4, polydispersity 1.6.

(d) N-Methyl-(4,4′-Bipyridinium) Hexafluorophosphate. 4,4′-Dipyridyl (5.0 g) was dissolved in methanol and purified by elution through a silica gel column. The solvent was removed under reduced pressure, and the solid was redissolved in acetonitrile. A stoichiometric amount of CH_3I was then added, and the solution was stirred at room temperature for 12 h. The solid product was collected by filtration, rinsed with acetonitrile, and then dissolved in water and converted to the PF_6^- salt by addition of excess aqueous $NH_4^+PF_6^-$. The product was collected by filtration, washed with water, and air-dried.

(e) Methyl Viologen-Functionalized PVT (PVT-MV^{2+}). PVTBr (0.2 g) was dissolved in $CHCl_3$ (100 mL). N-Methyl-(4,4′-bipyridinium)$^+PF_6^-$ (0.4 g, 1 mmol) was dissolved in CH_3CN (50 mL). The latter was then poured into the polymer solution, and the mixture was refluxed overnight. A yellow precipitate formed, which coated the inside of the flask. The solvent was poured off while still warm and the mixed-salt precipitate was dried under flowing air. To convert the mixed Br^-/PF_6^- salt to the Cl^- salt, the polymer was redissolved in acetone/water. HCl (1 M) was added, resulting in immediate precipitation. The precipitate was allowed to settle, and the solvent was poured off. The precipitate was dried under vacuum. ^{1}H NMR (CD_3OD) 4.5–4.7 (br, 2H, CH_3 and CH_2Br), 5.7–6.2 (br, 1.4H, CH_2), 6.2–7.5 (br, 4H, C_6H_4), 8.6–9.7 (d br, 4.4H, $C_{10}H_8N_2Cl_2$).

The chloride salt of PVT-MV^{2+} was converted to the PF_6^- salt in order to obtain a chlorine-free sample for analysis, and to prepare samples for cyclic voltammetry. The polymer was first dissolved in 10 mL CH_3OH, then an equal volume of water was added. Aqueous $NH_4^+PF_6^-$ was added to the solution until it became cloudy. Half of the solvent was then removed under reduced pressure, and the remaining mixture was centrifuged. The recovered solid was washed three times with water and dissolved in CH_3CN. The solvent was removed under reduced pressure and the precipitate was dried under vacuum. The product was stirred in water for 2 h to remove any entrained salts. The mixture was then filtered and dried under vacuum to yield PVT-MV^{2+}·$2PF_6^-$. The loading of viologen was estimated from ^{1}H NMR to be about 45%: ^{1}H NMR (CD_3CN) 4.2–4.6 (br, 1.9H, CH_3 and CH_2Br), 5.3–5.8 (br, 0.9H, CH_2), 6.1–7.4 (br, 4H, C_6H_4), 8.2–9.0 (d br, 3.6H, $C_{10}H_8N_2(PF_6)_2$). Elemental analysis was in reasonable agreement (39%) with this value. The composition was calculated with the assumption that the fraction of the polymer (44%) that was not brominated in the first step of the synthesis remained unreactive in the quaternization reaction. Calculated for $[C_9H_{10}]_{0.44}$-$[C_9H_9Br]_{0.17}$-$[C_{20}H_{21}N_2P_2F_{12}]_{0.39}$ (formula weight 311, equivalent weight 797): C, 51.3; H, 4.42; N, 3.51; Br, 4.36. Found: C, 49.9; H, 4.24; N, 3.59; Br, 4.36.

3. Growth and Characterization of Polyelectrolyte Multilayers.
(a) Preparation of Planar Substrates. Polished Si (100) wafers (p-type, $3.5–9.5 \times 10^{15}$ cm^{-3} carrier concentration, resistivity 1.5–4 Ω-cm) were obtained from Research and PVD Materials Company, and cut into rectangles using a diamond scribe. Borosilicate glass microscope cover slips (Fisher) and silicon wafers were sonicated in CCl_4 for 15 min and rinsed with methanol and water. They were then sonicated in 3:1 v/v concentrated H_2SO_4, 30% H_2O_2 (piranha) solution for 30 min and rinsed with water, methanol, methanol/toluene (1:1 v/v), and toluene before being derivatized in a 0.05 wt % solution of (4-aminobutyl)dimethylmethoxysilane in toluene for 12 h. Samples containing PVT-MV^{2+} layers were made on quartz microscope cover slips (Chemglass) and were agitated by swirling instead of sonication. The derivatized substrates were then rinsed with toluene, methanol/toluene, methanol, and water, and were immediately immersed into the exfoliated α-ZrP or HTiNbO$_5$ suspension (see below).

(b) Preparation of Amine-Derivatized Fumed Silica. M-5 scintillation grade Cab-O-Sil fumed silica (Acros Organics) was derivatized by suspending 5.0 g in 300 mL dry toluene, purging with argon for 15 min, and vigorously stirring in a sealed Teflon container with 0.5 mL (4-aminobutyl)dimethylmethoxysilane. After 12 h, the mixture was centrifuged and the silica particles were rinsed in toluene, methanol/toluene (1:1), methanol, and water. During each rinse step the suspension was stirred vigorously for 20 min and then centrifuged to collect the solid.

(c) Exfoliation of α-Zr(HPO$_4$)$_2$·H_2O (α-ZrP) and HTiNbO$_5$. Colloidal suspensions of α-ZrP were prepared by adding 1.24×10^{-4} mol tetra(n-butylammonium) hydroxide (TBA$^+OH^-$) to 1.66×10^{-4} mol α-ZrP in 25 mL Nanopure water, and stirring for 1 h. The reaction was carried out at ice bath temperature in order to minimize base hydrolysis of the colloid.[21] The pH of the colloid was 9.5–10. Ten milligrams (4.5×10^{-5} mol) HTiNbO$_5$[19] was suspended in 25 mL Nanopure water. Colloidal suspensions were prepared by dropwise addition of 40% TBA$^+OH^-$, until the pH had stabilized at 9.5–10 for at least 1 h.

(d) Assembly of Multilayer Films. The sequential adsorption of polycations and polyanions was carried out at 0 °C, using general procedures described previously.[18] Typically, chromophore-PAH and the porphyrin layers were deposited from 10 mM and 10 μM solutions, respectively, at pH 7–7.5. PVT-MV^{2+} polymer layers were made from 15 meq/L solutions of the chloride salt in methanol. The inorganic spacer layers, α-ZrP or HTiNbO$_5$, were made from 6.4 and 2 meq/L aqueous suspensions, respectively. All adsorption times were 10 min for the glass and quartz substrates, and 20–30 min for the fumed silica substrates, both with copious water rinses between each deposited layer. After each adsorption step, a portion of the silica samples was set aside for CHN analysis, inductively coupled plasma–atomic emission spectroscopy (ICP–AES) analysis for Zr and Ti, surface area measurements, and transmission electron microscope (TEM) analysis.

After thorough rinsing with water, 0.07 g of the derivatized silica was immediately stirred for 20–30 min in 40 mL of the exfoliated α-ZrP suspension. The silica/amine/α-ZrP sample was then centrifuged, rinsed three times with water, and stirred in a 15 mM solution of the chloride salt of the PVT-MV^{2+} polymer in methanol for 20–30 min. The samples were then centrifuged and rinsed, as described above, until there was no detectable UV absorbance of the viologen polymer in the supernatant rinse solutions (typically three to five rinse/centrifuge cycles were needed). The loading of the PVT-MV^{2+} polymer on silica was determined by drying the sample at 110 °C for 24 h, digesting it in 1% HF, and measuring the 260 nm UV absorbance of the resulting solution. An extinction coefficient of 22 600 was obtained for the PVT-MV^{2+} polymer in 1% aqueous HF from a Beer's Law plot. This value is in reasonable agreement with the literature value of 20 700[22] for MV^{2+} in water. Viologen coverages calculated from the difference in 260 nm absorbances of the supernatant solutions before and after the layer was grown typically agreed within 10%; however, the latter method was not routinely used for analysis because some light scattering was observed, even after extensive centrifugation of the silica suspensions.

The silica/amine/α-ZrP/PVT-MV^{2+} sample was stirred in 40 mL of the exfoliated α-ZrP or HTiNbO$_5$ suspension for 30 min, and then

(21) Kaschak, D. M.; Johnson, S. A.; Hooks, D. E.; Kim, H.-N.; Ward, M. D.; Mallouk, T. E. *J. Am. Chem. Soc.* **1998**, *120*, 10887.
(22) Watanabe, T.; Honda, K. *J. Phys. Chem.* **1982**, *86*, 2617.

rinsed/centrifuged three to five times. These silica/amine/ZrP/PVT-MV^{2+}/(ZrP or $HTiNbO_5$) samples were stirred in a 10 mM aqueous PAH at pH 7 for 30 min, and rinsed/centrifuged in the usual manner. The resulting composites were then stirred in a 10 μM $PdTSPP^{4-}$ solution at pH 7 for 30 min and rinsed with water. A portion of sample was again digested in 1% aqueous HF, and the loading of porphyrin molecules was determined by UV−vis spectroscopy.

4. Instrumentation. Descriptions of instruments and procedures used for ellipsometry, TEM, atomic force microscopy (AFM), and cyclic voltammetry are given in the Supporting Information section.

(a) Steady-State Absorption and Emission Spectroscopy. Transmission UV−vis absorption spectra were acquired on a Hewlett-Packard HP8452A diode array spectrometer. Diffuse reflectance UV−vis spectra were obtained from suspensions with a Varian DMS 300 instrument. Steady-state emission spectra were taken on a SPEX Fluorolog 1680 0.22 m double monochromator fluorimeter using a front face illumination and collection geometry. The emission spectra were corrected for the instrument response as they were obtained. Films were grown on both sides of the glass substrates, and all absorption/emission spectra therefore reflect a doubled absorption or emission relative to a one-sided sample. UV−vis absorption spectra of multicomponent samples on glass slides were deconvoluted using reference monolayer spectra. In general, the spectra were quite reproducible with identically prepared samples, but the amount of a dye adsorbed depended on the sequence of adsorption steps. Therefore, the individual components of the deconvoluted absorption spectra were used to normalize the emission intensities. Details of the procedure, and of the calculation of Förster radii, are given in the Supporting Information section.

(b) Time-Resolved Spectroscopy. Laser flash photolysis/transient diffuse reflectance experiments were carried out on high surface area samples, using a system similar to that described previously.[19] Details are given in the Supporting Information section. Typical flash photolysis samples consisted of 0.063 g of the silica composite suspended in 3.0 mL Nanopure water. Diffuse reflectance UV−vis spectra of each sample were compared to a reference sample of composition silica/amine/ZrP/PAH/PdTSPP.[4−] Small sample-to-sample differences in scattering or in the $PdTSPP^{4-}$ loading were compensated for by adding 0.0−0.1 mL deionized water to the sample or to the reference, until the diffuse reflectance maxima at the laser wavelength (532 nm) were identical. Approximate quantum yields for photoinduced electron transfer were obtained by comparing transient signals with those of an "actinometer" sample. The latter consisted of an identically prepared multilayer composite, which contained the same loading of $PdTSPP^{4-}$ but no PVT-MV^{2+} electron acceptor. This procedure compensates for scattering, reflection from the sample cuvette, and related instrumental parameters. All quantum yields reported herein represent averages of at least two independently prepared samples. Typically, the relative error in these measurements inferred from duplicate experiments was ±10%.

Results and Discussion

Spectral Properties of Photon Antenna and Photoredox Molecules. Efficient Förster energy transfer in a supramolecular assembly requires good spectral overlap between donor emission and acceptor absorption spectra. Ideally, one would like to assemble a series of molecules that together make a "black absorber" across the visible region of the spectrum. Energy transfer from the bluest to progressively redder absorbers should funnel excitation to a redox-active trap molecule.

Scheme 1 summarizes the structures and spectral characteristics of the molecules used in this study. The coumarin polymer (Coum-PAH) absorbs in the blue region of the visible spectrum ($\lambda_{max} = 412$ nm), and its emission maximum, 485 nm, coincides with the intense absorption band of the fluorescein polymer Fl-PAH ($\lambda_{max} = 500$ nm). The Coum-PAH emission also overlaps to some extent with the Q-band absorptions of porphyrin molecules $PdTAPP^{4+}$ and $PdTSPP.^{4-}$ The emission maximum of Fl-PAH (530 nm) is essentially coincident with the porphyrin Q-band absorbance maximum. In addition, the porphyrins have

Scheme 1. Energy and Electron Transfer Pathways (Indicated by Arrows) for the Energy "Antenna" Polymers, Coum-PAH and Fl-PAH; the Photosensitizers, $PdTAPP^{4+}$ and $PdTSPP;^{4-}$ and the Electron Acceptor Polymer, PVT-MV^{2+}.
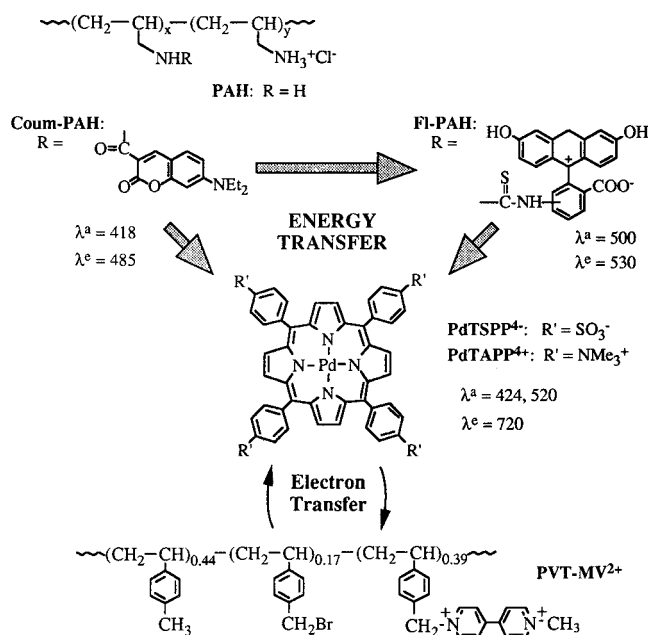
Scheme 2. Possible Architectures for Photoinduced Intra- (left) and Interlayer (right) Energy Transfer Followed by Interlayer Electron Transfer.
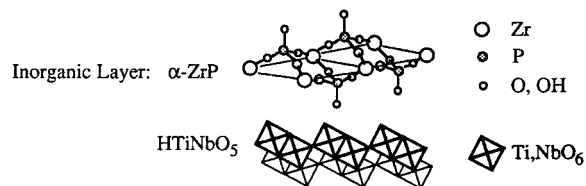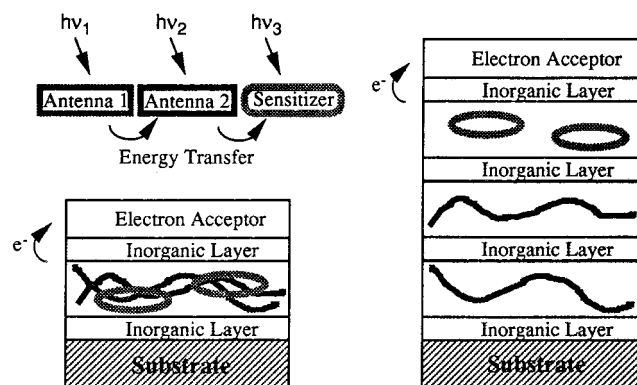
a strong Soret absorption band slightly to the red of the Coum-PAH absorbance maximum. Together the three chromophores are strongly absorbing across the short wavelength region of the visible spectrum, between 380 and 550 nm. The PVT-MV^{2+} polymer does not absorb in the visible, and therefore cannot participate in the energy transfer cascade. However, the viologen groups in this polymer are capable of accepting an electron from either the singlet or triplet excited state of the porphyrin molecules.[23]

The Coum-PAH → Fl-PAH → porphyrin energy transfer cascade must be fast for the system to function efficiently,

(23) Okura, I.; Aono, S.; Takeuchi, M.; Kusunoki, S. *Bull. Chem. Soc. Jpn.* **1982**, *55*, 3637.
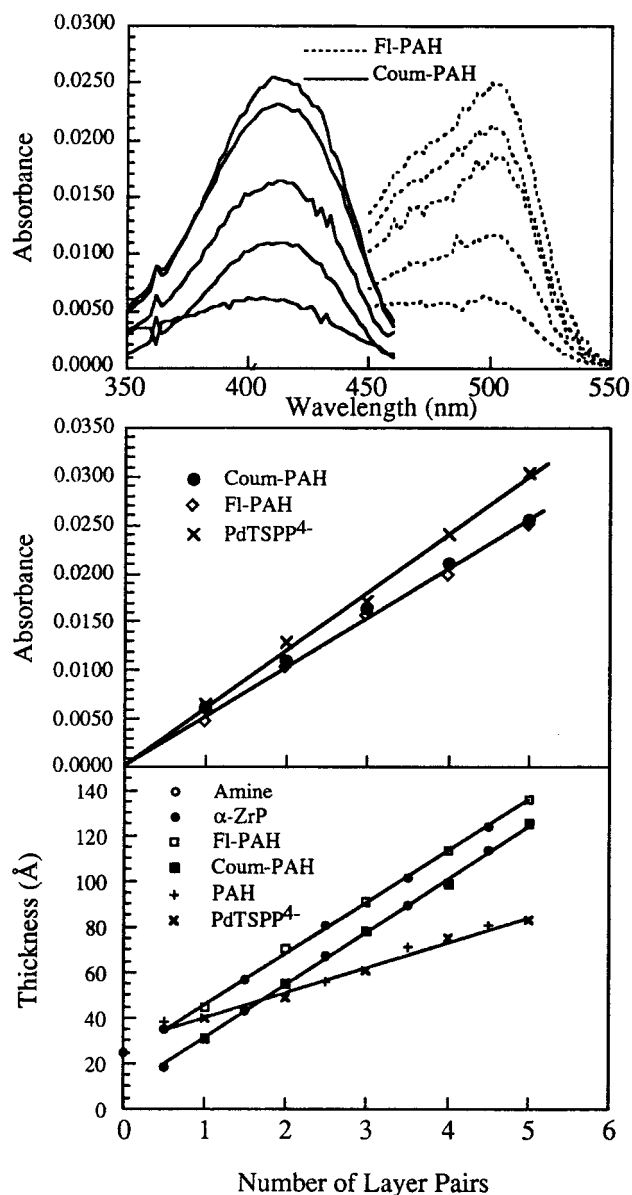
Figure 1. Top: UV−vis spectra of five sequentially adsorbed α-ZrP/dye−PAH layer pairs (dye = Coum, Fl) on glass/amine substrates. Middle: Absorbance at λ_{max} vs number of bilayers for α-ZrP/dye−PAH and PdTSPP^{4-}/PAH multilayer sequences. Bottom: Ellipsometric film thickness (Å) vs number of layer pairs for films grown on silicon. Zero layers corresponds in each case to the amine-derivatized substrate.

because of the short singlet excited-state lifetimes ($\tau_{coum} \sim 3$ ns,[24] $\tau_{Fl} \sim 4$ ns[25]) of the coumarin and fluorescein dyes. The presence of a Pd atom in the porphyrins ensures quantitative intersystem crossing to a long-lived triplet excited state, which allows ca. 100−200 μs for the porphyrin → viologen electron-transfer step to occur.[26] In addition, the triplet state porphyrins show room-temperature phosphorescence, allowing one to monitor the forward electron-transfer reaction by emission spectroscopy.

Scheme 2 shows the two kinds of multilayer structures that were prepared for studying intra- and interlayer energy and electron transfer reactions. In one, the Coum-Fl−porphyrin energy transfer cascade is sequentially adsorbed or coadsorbed
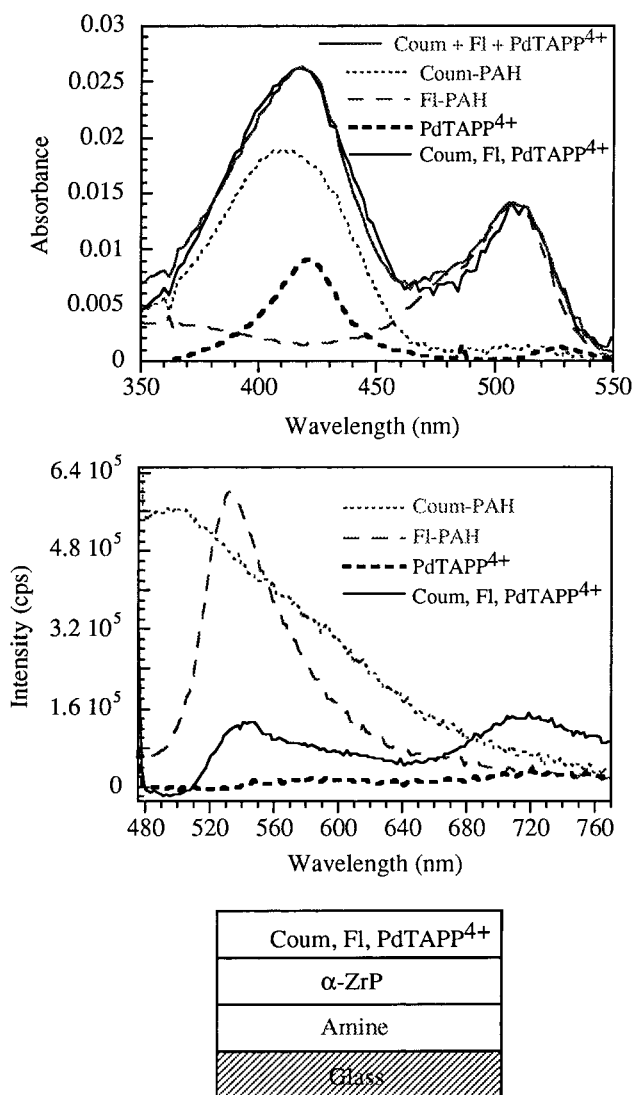
(24) Jones, G., II; Jackson, W. R.; Choi, C.-Y.; Bergmark, W. R. *J. Phys. Chem.* **1985**, *89*, 294.

(25) Fairclough, R. H.; Cantor, C. R. In *Methods in Enzymology*; Academic Press: New York, 1977; p 363.


Figure 2. UV−vis absorption (top) and steady-state emission (bottom, $\lambda_{ex} = 450$ nm) spectra of individual chromophore layers (Coum-PAH, Fl-PAH, and PdTAPP^{4+}) and of the coadsorbed triad Coum-PAH, Fl-PAH, PdTAPP^{4+} on glass/amine/α-ZrP. The summed absorbances of the individual chromophores (Coum-PAH + Fl-PAH + PdTAPP^{4+}) match the absorbance of the coadsorbed triad.

between a pair of polyanion sheets. In the other, each component is confined to its own layer, and energy transfer occurs across the spacers (α-ZrP or HTiNbO$_5$). The electron acceptor polymer, PVT-MV^{2+}, should be confined to its own layer in either case, to inhibit the back electron-transfer reaction to the porphyrin sensitizer. Previous work showed that there is minimal interpenetration of polymer layers in lamellar assemblies of this kind, and that the average interlayer spacing of dye−PAH/α-ZrP bilayer is ca. 22 Å.[17]

Growth and Characterization of Polyelectrolyte Multilayer Films. Multilayer thin films of the derivatized PAH polycations, porphyrin anions/cations, and inorganic polyanions (α-ZrP and HTiNbO$_5$) were prepared by alternate anion/cation adsorption reactions. The adsorption process is self-limiting, and monolayer formation is complete within the 10 min allowed for each step. Figure 1 shows UV−vis absorption spectra and ellipsometric data for α-ZrP/dye−PAH and PdTSPP^{4-}/PAH layer pairs grown on glass. The thickness changes per layer pair were 23, 22, and 9 Å, and the absorbance changes indicate that 5.3, 4.8, and 2.7 × 10^{-11} mol/cm^2 of the Coum, Fl, and PdTSPP^{4-} chromophores, respectively, are deposited in each
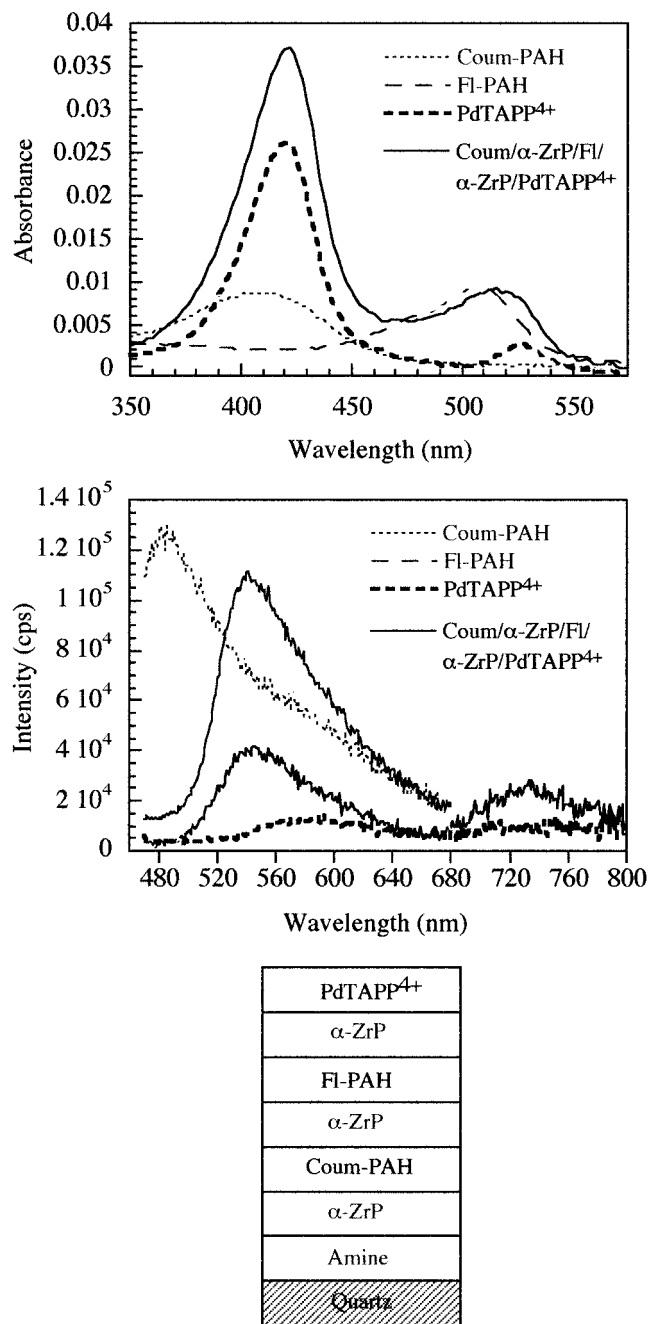
Figure 3. Absorption (top) and emission (bottom, $\lambda_{ex} = 450$ nm) spectra of the individual chromophore layers and the multilayer triad containing Coum-PAH, Fl-PAH, and PdTAPP^{4+}. Chromophore poly-cation layers are separated by α-ZrP sheets.

adsorption cycle. Both the absorbance and thickness changes are linear with layer number, although the intercept of the ellipsometric plot varies from sample to sample. Recalling that the loading of Coum and Fl dyes is 1/40−1/50 per PAH monomer unit, the PAH coverage is ca. 2×10^{-9} mol/cm^2, or 1 per 8 Å^2. This is roughly three times the density of ion exchange sites on the flanking α-ZrP sheets (1 per 24 Å^2), and is consistent with the fact that the PAH amine groups are partly deprotonated at pH 7.0−7.5. Each dye−PAH layer adds 10−12 Å to the total film thickness, compared to 6 Å for PAH deposited at pH 5,[18] indicating that the polymer chain is partially coiled rather than fully extended at neutral pH. The adsorption of each α-ZrP layer adds 10−12 Å to the film thickness. The 22 Å thickness per α-ZrP/dye−PAH layer pair is close to the Förster radii calculated for the different donor−acceptor com-
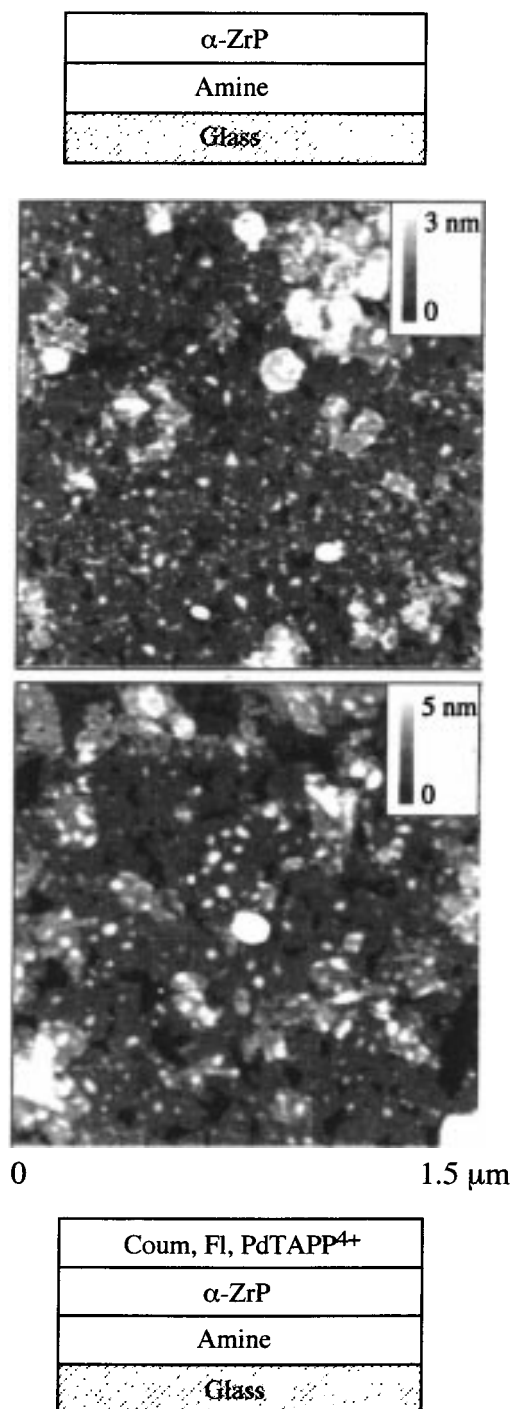

Figure 4. Tapping mode AFM images of α-ZrP and α-ZrP/coadsorbed triad samples on glass/amine substrates.

binations (22, 16, and 19 Å for the Coum-Fl, Coum-porphyrin, and Fl-porphyrin dyads, respectively).

Energy Transfer in Coumarin-Fluorescein-PdTAPP^{4+} Triads. Figure 2 shows absorption and emission spectra for an energy transfer assembly containing coadsorbed Coum-PAH, Fl-PAH, and PdTAPP^{4+} on a glass/amine/α-ZrP substrate, and Figure 3 shows similar spectra from a sequentially adsorbed sequence of the same dyes with intervening α-ZrP layers. AFM images of the coadsorbed sample are shown in Figure 4. Gray areas in the top image, at an average height of 12 Å above the glass/amine background, correspond to unilamellar α-ZrP sheets. These sheets cover most of the surface, although there are patches (white) of sheet bilayers and other "surface junk."

Table 1. Comparison of the Energy and Electron Transfer Quantum Yields in Different Donor−Acceptor Sequences

			coverage (mol/cm²) × 10¹¹			
	χ measured (calc.)	figure	Coum	Fl	porphyrin	MV²⁺
Coadsorbed System: (Substrate: Borosilicate/amine/α-ZrP)						
Coum, Fl, PdTAPP⁴⁺	0.82 (0.70)	2	14	9.1	3.3	
Layered Systems: (Substrate: Quartz/amine/α-ZrP)						
Coum/α-ZrP/Fl/α-ZrP/PdTAPP⁴⁺	0.65 (0.62)	3	8.8	6.3	5.1	
Coum/α-ZrP/Fl	0.79 (0.71)					
Fl/α-ZrP/PdTAPP⁴⁺	(0.83)					
Coum/α-ZrP/PdTAPP⁴⁺	(0.03)					
Coum/PdTSPP⁴⁻/Fl/α-ZrP/PVT-MV²⁺	0.47[a] (0.42)	5	5.5	4.2	0.8	2.2
Coum/PdTSPP⁴⁻/Fl	0.81 (0.70)					
PdTSPP⁴⁻/PAH/α-ZrP/PVT-MV²⁺	0.58[a]					
Coum/PdTSPP⁴⁻	(0.22)					
Coum,Fl	(0.94)					
PdTSPP⁴⁻/Fl	(0.44)					
Coum/PdTSPP⁴⁻/Fl/HTiNbO₅/PVT-MV²⁺	0.61[a] (0.58)	6	5.0	3.5	1.3	3.5
Coum/PdTSPP⁴⁻/Fl	0.80 (0.75)					
PdTSPP⁴⁻/PAH/HTiNbO₅	0.55[a]					
PdTSPP⁴⁻/PAH/HTiNbO₅/PVT-MV²⁺	0.76[a]					
High surface area samples: (substrate: silica, "///": silica/amine/α-ZrP)						
///PVT-MV²⁺/α-ZrP/PAH/PdTSPP⁴⁻	0.17[b]	9			0.17	8.8
///PVT-MV²⁺/HTiNbO₅/PAH/PdTSPP⁴⁻	0.30[b]	9			0.23	12
	0.99[b]					

[a] Energy/electron-transfer quantum yield measured by steady-state emission spectroscopy. [b] Charge separation yield measured by laser flash photolysis/transient diffuse reflectance.

Addition of the coadsorbed dye layer does not change the overall appearance of the AFM image, except that the height of the sheets above the background is 24 Å. The additional 12 Å thickness is consistent with the ellipsometric data for dye−PAH layers shown in Figure 1.

The triad absorption spectra in Figures 2 and 3 are accurately reproduced by adding together the appropriately scaled mono-layer absorption spectra. However, emission spectra obtained by exciting into the coumarin absorption band (λ_{ex} = 450 nm) show evidence of efficient energy transfer. There is nearly complete quenching of the coumarin emission at 485 nm, substantial quenching of fluorescein emission at 530 nm, and greatly enhanced porphyrin emission at 720 nm, relative to reference spectra of the individual components excited at 450 nm.

Table 1 summarizes the coverages of each of the dyes, and the energy transfer quantum yields in the two triad assemblies. For the coadsorbed triad, the average intermolecular distances are significantly less than the Förster radii, and therefore the energy transfer process is very efficient (χ = 0.82). For the multilayer sample, the process is less efficient (χ = 0.65), because of the increased average distance between chromophores. The energy transfer quantum efficiencies in the bilayer dyad Coum-PAH/α-ZrP/Fl-PAH and in the triad multilayer are both reproduced accurately by Monte Carlo simulations that assume random $x-y$ coordinates of the dye molecules and minimal interpenetration of polyelectrolyte layers (Table 1).

Energy and Electron-Transfer Reactions in Coum-PAH, PdTSPP⁴⁻, Fl-PAH/Spacer/PVT-MV²⁺ Systems. The addition of an α-ZrP/PVT-MV²⁺ bilayer to the triad systems described above results in minimal changes in the emission spectra. Transient absorbance spectra of PVT-MV²⁺/α-ZrP/PdTAPP⁴⁺ on silica supports showed features that could be assigned to the triplet excited state of the porphyrin, and no transients characteristic of reduced viologen groups. In this case, electron transfer from ³PdTAPP⁴⁺ to PVT-MV²⁺ is slow because of the weak driving force ($\Delta G°$ = +0.05 eV)[26] for the reaction. It is, however, possible to accelerate this reaction by using anionic

metalloporphyrins, which are better reducing agents than their cationic relatives.[27] The formal potential of ³PdTSPP⁴⁻ is −0.77 V vs saturated calomel electrode (SCE), about 0.3 V more negative than that of ³PdTAPP⁴⁺. This provides ample driving force for electron transfer within the triplet excited-state lifetime of the porphyrin, across the 1 nm-thick α-ZrP spacer.

Figures 5 and 6 show composite absorption and emission spectra of films in which the energy transfer triad is coupled to a viologen polymer layer. In this case, the cation/anion adsorption sequence was Coum-PAH/PdTSPP⁴⁻/Fl-PAH/spacer sheet (α-ZrP or HTiNbO₅)/PVT-MV²⁺. Decher and co-workers showed that unbranched polyelectrolytes such as PAH and poly-(styrenesulfonate) interpenetrate substantially when they are sequentially adsorbed.[15] The high quantum efficiency of energy transfer within the triad (χ = 0.81, Table 1) is consistent with mixing or even clustering of the three dye molecules. This idea is supported by Monte Carlo simulations, which underestimate the quantum efficiency (χ = 0.70) when the three dye molecules are placed at random $x-y$ positions in the interlayer gallery. On the other hand, there is little or no interpenetration of dye layers that are separated by the inorganic sheets.[17,28] α-ZrP and HTiNbO₅ sheets, which tile the cationic surface quite densely (as shown by AFM images in Figures 4 and 7, respectively), therefore enforce a minimum separation of 1 nm between the porphyrin and viologen molecules.

The addition of a spacer/PVT-MV²⁺ bilayer to the Coum-PAH/PdTSPP⁴⁻/Fl-PAH triad results in efficient quenching of the porphyrin phosphorescence at 720 nm. From the change in emission intensity, electron-transfer quantum yields of 0.58 and 0.76 are found for the α-ZrP and HTiNbO₅ spacers, respectively. Interestingly, the HTiNbO₅ spacer alone (without PVT-MV²⁺) contributes to quenching of the porphyrin excited state, as evidenced by the lower phosphorescence intensity of Coum-PAH/PdTSPP⁴⁻/Fl-PAH/HTiNbO₅, relative to Coum-PAH/PdTSPP⁴⁻/Fl-PAH (Figure 6). This shows that the titanoniobate

(26) Brun, A. M.; Harriman, A. *J. Am. Chem. Soc.* **1994**, *116*, 10383.

(27) Harriman, A.; Richoux, M. C.; Neta, P. *J. Phys. Chem.* **1983**, *87*, 4957.

(28) Kerimo, J.; Adams, D. M.; Barbara, P. F.; Kaschak, D. M.; Mallouk, T. E. *J. Phys. Chem. B* **1998**, *102*, 9451.
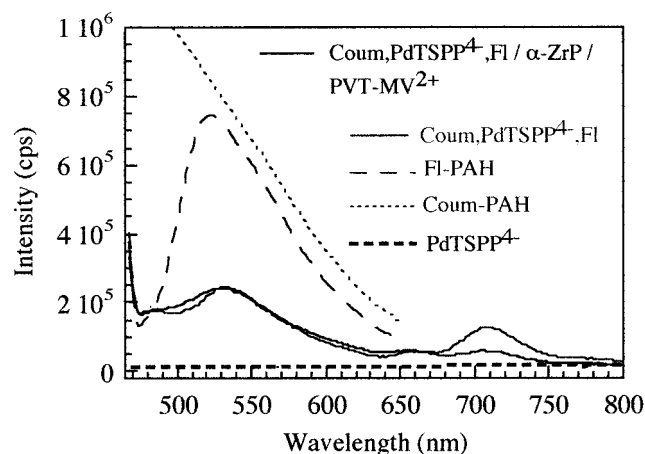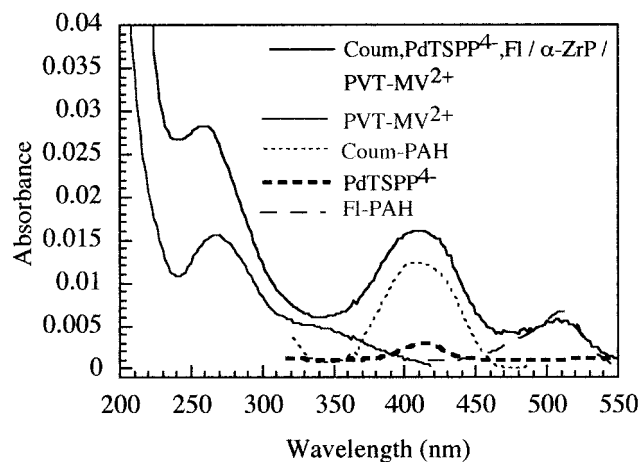
Figure 5. Absorption (top) and emission (bottom, λ_{ex} = 450 nm) spectra of an energy/electron transfer assembly with α-ZrP spacer separating the porphyrin and viologen layers. Dotted lines in the idealized picture at the right indicate a mixed Coum-PAH, PdTSPP^{4-}, Fl-PAH polyelectrolyte layer. Reference spectra from individual chromophore layers (Coum-PAH, PdTSPP^{4-}, Fl-PAH) and from the triad without PVT-MV^{2+} are also shown. As in Figures 2 and 3, the Coum-PAH, PdTSPP^{4-}, Fl-PAH triad shows decreased Coum (485 nm) and Fl (530 nm) fluorescence, and increased PdTSPP^{4-} phosphorescence (720 nm). Addition of a PVT-MV^{2+} polymer layer quenches the PdTSPP^{4-} phosphorescence.

sheets, in addition to providing a spacer between electron donor and acceptor layers, can themselves accept an electron from ^{3}PdTSPP.$^{4-}$ Overall, the combined energy/electron-transfer cascades have quantum yields of 0.47 and 0.61 with α-ZrP and HTiNbO$_5$ spacers, respectively (Table 1).

Photoinduced Electron Transfer in Multilayer Films on High Surface Area Silica. The steady-state luminescence experiments described above support the model of sequential energy and electron-transfer steps, as sketched in Scheme 1. However, steady-state experiments are not very informative about the dynamics of these reactions. Furthermore, they give
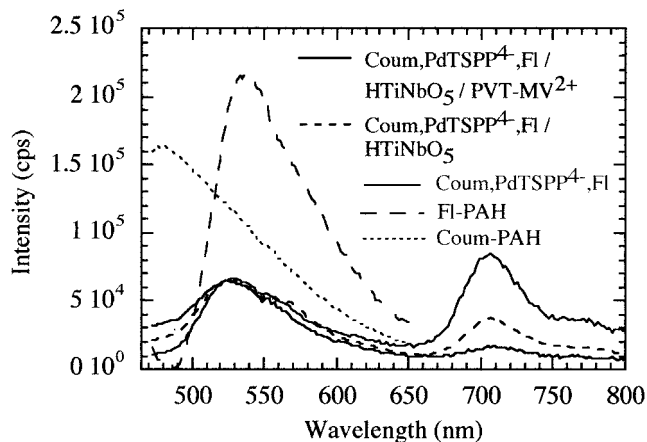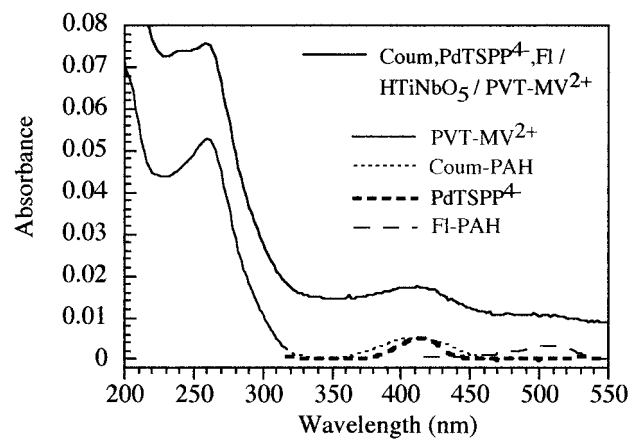
Figure 6. Absorption (top) and emission (bottom, λ_{ex} = 450 nm) spectra of the same energy/electron transfer assembly shown in Figure 5, but with HTiNbO$_5$ replacing α-ZrP as the spacer between porphyrin and viologen layers.

no information about the fate of the oxidized porphyrin − reduced viologen charge separated state that results from excitation of the coumarin antenna chromophore. To gain more insight into these questions, multilayer films were grown on high surface area silica supports. Although these high surface area supports are not amenable to characterization by ellipsometry or AFM, they provide sufficient optical density to obtain transient spectra in diffuse reflectance mode.

Because the primary silica particles are small (∼50 nm) relative to the lateral dimensions of the HTiNbO$_5$ sheets (2−5 μm), the multilayer films are expected to be morphologically different from those grown on planar supports. Figure 8 shows TEM images of the silica particles at various stages of layer growth. There is progressive agglomeration of the silica particles with addition of polyelectrolyte layers, especially when the large HTiNbO$_5$ sheets are added (Figure 8d). This is consistent with the trend toward lower Brunauer−Emmett−Teller (BET) surface area (Table 2). The particle agglomerates also become increasingly opaque in the TEM as more layers are added, again
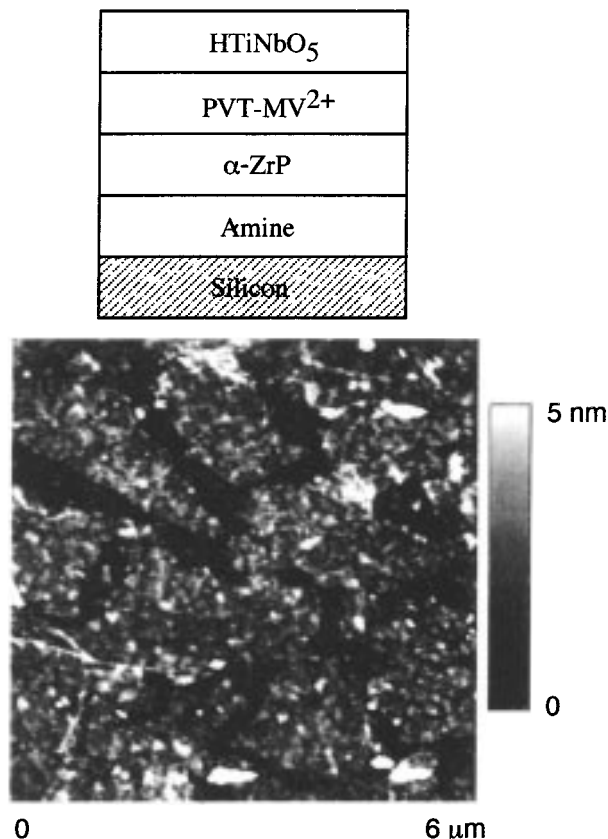
Figure 7. Tapping mode AFM image of HTiNbO$_5$ sheets on a glass/amine/α-ZrP/PVT-MV^{2+} substrate.

Table 2. Elemental and BET Surface Area Analysis of Silica/Polymer/Sheet Composites[a]

	%C	%H	%N	BET surface area (m^2/g)
silica	0.24	0.25	0.00	200
silica/amine	1.39	0.35	0.06	180
silica/amine/α-ZrP	2.38	0.61	0.19	150
silica/amine/α-ZrP/PVT-MV^{2+}	5.42	0.78	0.42	150
///PVT-MV^{2+}/HTiNbO$_5$	6.08	0.65	0.42	150
///PVT-MV^{2+}/HTiNbO$_5$/PAH	5.92	0.69	0.59	150
///PVT-MV^{2+}/HTiNbO$_5$/PAH/ PdTSPP^{4-}	7.45	0.61	0.52	140

[a] "///" denotes a silica/amine/α-ZrP substrate.

consistent with the idea of sequential polyanion/polycation adsorption (Scheme 2).[16] However, the TEM images of the agglomerated particles do not resolve the individual sheets sufficiently to give information about the detailed structure of the multilayers.

Elemental analysis shows that silanization of the silica surface with 4-(aminobutyl)dimethylmethoxysilane adds 1% C to the samples. From the carbon content and the surface area of the underivatized silica (200 m^2/g), the density of amine groups on the surface is calculated to be 8×10^{-11} mol/cm^2. Adsorption of α-ZrP sheets adds 2.6% Zr, or a Zr(HPO$_4$)$_2$ coverage of 2×10^{-10} mol/cm^2. This is roughly consistent with adsorption of a single layer of α-ZrP (24 Å^2/Zr = 7×10^{-10} mol/cm^2), allowing that much of the area of the agglomerated particles is inaccessible to the sheets. The α-ZrP adsorption step also affects the carbon content, as expected from coadsorption of TBA$^+$ cations. The 1% C increase gives a TBA$^+$ coverage of 3×10^{-11} mol/cm^2, which can be compared to the amount needed (1×10^{-10} mol/cm^2) to completely cover one side of the α-ZrP sheets. Adsorption of PVT-MV^{2+} layer adds another 4% C (assuming

that TBA$^+$ is completely displaced), or 1.5×10^{-10} mol/cm^2 of viologen groups. This is in good agreement with the viologen loading (1.0×10^{-10} mol/cm^2) calculated from UV−vis spectra of composites dissolved in 1% HF, and is also consistent with the amount of charge needed to compensate the flanking α-ZrP and HTiNbO$_5$ (7×10^{-11} mol/cm^2, 0.46% Ti) layers.

PdTSPP^{4-} was adsorbed quantitatively onto silica/amine/α-ZrP/PVT-MV^{2+}/spacer/PAH composites from solutions that contained fewer moles than needed to make a full monolayer. Typically, the PdTSPP^{4-} coverage was kept at about 2×10^{-12} mol/cm^2. This ensures that under conditions of laser excitation (in which most of the porphyrin molecules are excited) there is a substantial molar excess of viologen electron acceptor molecules.

There are obvious differences between the structure of multilayer films grown on planar supports and high surface area silica, and therefore comparisons between the two must be made cautiously. Nevertheless, the same basic trends are observed for the two kinds of samples. In particular, quenching of the porphyrin triplet excited state is more efficient in composites containing titanoniobate spacers than α-ZrP spacers. Transient spectroscopy of the high surface area composites provides information about the dynamics of the forward and back electron-transfer processes that is not accessible with the planar samples. Figure 9 shows diffuse reflectance transients and spectra for the PVT-MV^{2+}/spacer/PAH/PdTSPP^{4-} electron-transfer dyad, in which the spacer layer is α-ZrP or HTiNbO$_5$, and kinetic data are collected in Table 3. The porphyrin is excited by a 15 ns, 532 nm laser flash, and rapid electron transfer to the viologen polymer occurs, as evidenced by the decay of the ^{3}PdTSPP^{4-} transient at 450 nm. On the time scale shown, the triplet transient from the control sample containing no PVT-MV^{2+} decays very slowly, and provides a useful transient "actinometer" for the other experiments.[29] By comparison, the samples containing PVT-MV^{2+} show fast, biexponential decays. The time constant of the fast, major component is 1.8−2.0 μs, and is the same within experimental error for both α-ZrP and HTiNbO$_5$ spacers. Both samples also appear to have a quenching component that is static (<50 ns) on the instrumental time scale. In this case, there is a significant difference between the two spacers, with more extensive static quenching by the HTiNbO$_5$ sample.

On longer time scales, 380 and 600 nm positive transients that can be attributed to the reduced viologen polymer PVT-MV$^{+\cdot}$ are observed (Figure 9, bottom).[30] The oxidized porphyrin cannot be directly observed because of its low extinction coefficient (3.0×10^3 M^{-1}cm^{-1})[29] and its spectral overlap with the more strongly absorbing reduced viologen at 600 nm. By comparing the 450 nm transient of the PdTSPP^{4-} actinometer with the 380 nm transient of the reduced viologen, and taking into account the ratio of extinction coefficients and spectral scattering correction, the quantum yields for charge separation were estimated to be 0.17 and 0.30 for α-ZrP and HTiNbO$_5$ spacers, respectively.

Interestingly, the charge recombination kinetics are quite different with the two spacers. With α-ZrP, the reduced viologen transients at 380 and 600 nm decay by first-order kinetics with a lifetime of 150 ± 10 μs. This can be interpreted as simple back electron transfer in the porphyrin−viologen dyad, through the "passive" α-ZrP spacer. On the other hand, the decays with the HTiNbO$_5$ spacer are biexponential (τ = 52, 900 μs). For

(29) Nahor, G. S.; Neta, P.; Hambright, P.; Thompson, A. N., Jr.; Harriman, A. *J. Phys. Chem.* **1989**, *93*, 6181.

(30) Neta, P.; Richoux, M.-C.; Harriman, A. *J. Chem. Soc., Faraday Trans. 2*, **1985**, *81*, 1427.
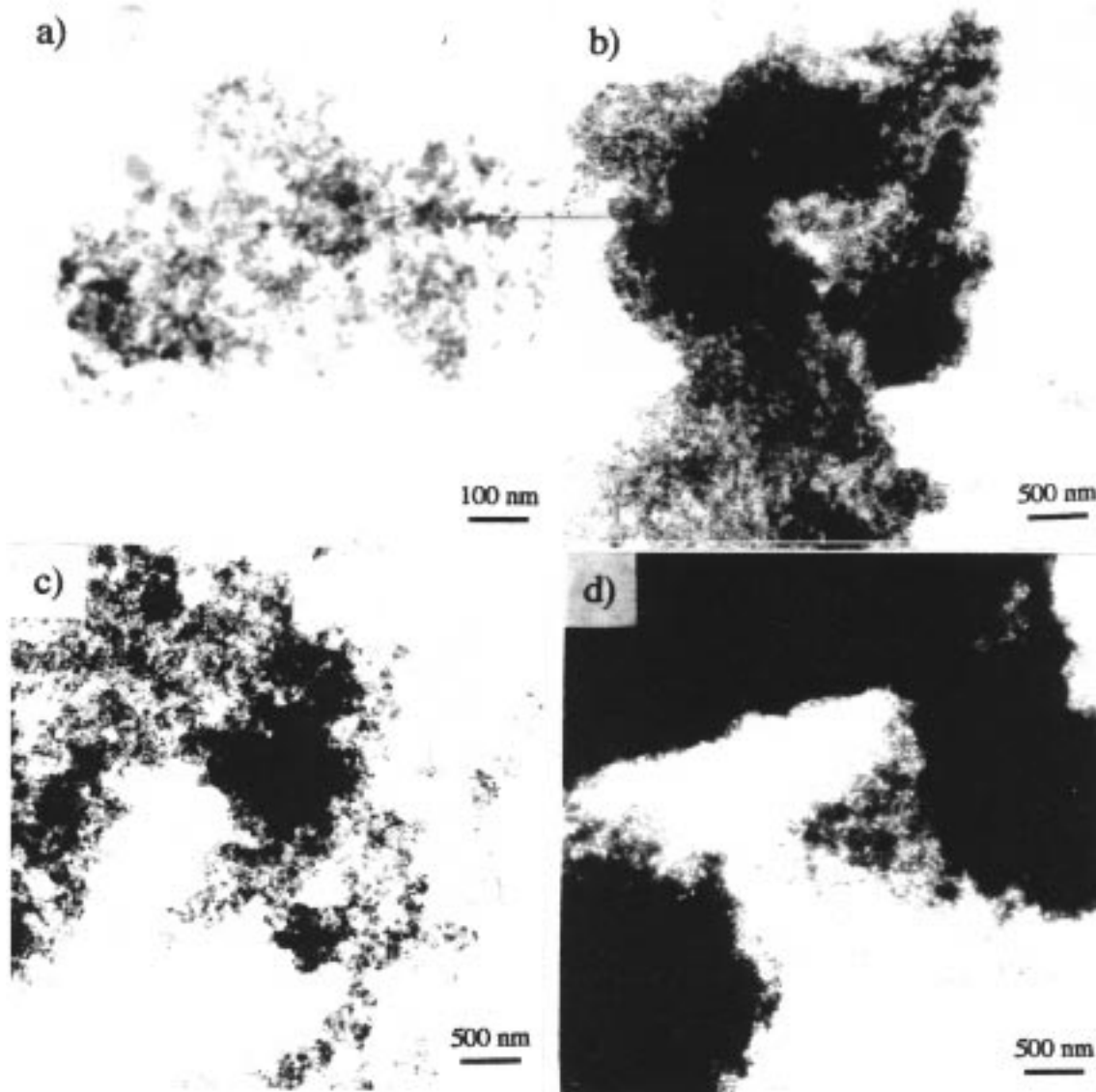
Figure 8. TEM images of silica composites containing: (a) amine, (b) amine/α-ZrP, (c) amine/α-ZrP/PVT-MV^{2+}, (d) amine/α-ZrP/PVT-MV^{2+}/HTiNbO$_5$.

Table 3.   Kinetic Parameters for the Data Fits Shown in Figure 9[a]

sample	A_1	τ_1	A_2	τ_2 (μs)
^{3}PdTSPP^{4-} decay at 450 nm				
///PVT-MV^{2+}/α-ZrP/PAH/PdTSPP^{4-}	0.0137(5)	83(1) ns	0.0062(5)	2.0(0.3)
///PVT-MV^{2+}/HTiNbO$_5$/PAH/PdTSPP^{4-}	0.0113(5)	58(3) ns	0.0049(3)	1.8(0.2)
///PAH/α-ZrP/PAH/PdTSPP^{4-}	0.0145(3)	14.5(4) μs		
MV^{2+}·decay at 600 nm				
///PVT-MV^{2+}/α-ZrP/PAH/PdTSPP^{4-}	0.0037(2)	150(10) μs		
///PVT-MV^{2+}/HTiNbO$_5$/PAH/PdTSPP^{4-}	0.0051(4)	52(4) μs	0.0015(4)	900(30)

[a] Single and double exponential decays were fit to $Y = A\,e^{-x/\tau_1}$ and $Y = A_1\,e^{-x/\tau_1} + A_2\,e^{-x/\tau_2}$, respectively. Uncertainties in the last digit are indicated in parentheses.

the long-lived major component, the 5-fold enhancement in charge separation lifetime suggests that HTiNbO$_5$ somehow creates a greater distance between the oxidized porphyrin and reduced viologen molecules. However, this is not likely to be the result of a simple structural difference between the two spacers. The thickness (8 Å for α-ZrP, 10 Å for HTiNbO$_5$) and layer charge density are about the same in both cases. Further, an increase in donor—acceptor distance should reduce the forward electron-transfer rate as well, and the opposite trend is observed in the static quenching component (Figure 9, top).

A reasonable explanation for all of these observations is that the semiconducting HTiNbO$_5$ sheets play an active role in

mediating the forward electron-transfer reaction. Estimates of the flat-band potential of bulk HTiNbO$_5$ (−0.66 V vs SCE)[31] place it between the formal potentials of ^{3}PdTSPP^{4-} (−0.77 V) and PVT-MV^{2+} (−0.56 V). The HTiNbO$_5$ sheet is capable of accepting an electron from ^{3}PdTSPP^{4-}, and this is consistent with the increased static quenching component observed in the ^{3}PdTSPP^{4-} transient at 450 nm (Figure 9, top). Once in the sheet, the electron may be transferred to viologen acceptors that are near (short-lived back electron-transfer component) or far (long-lived component) from the oxidized porphyrin molecule.

(31) Kim, Y. I.; Atherton, S. J.; Brigham, E. S.; Mallouk, T. E. *J. Phys. Chem.* **1993**, *97*, 11802.
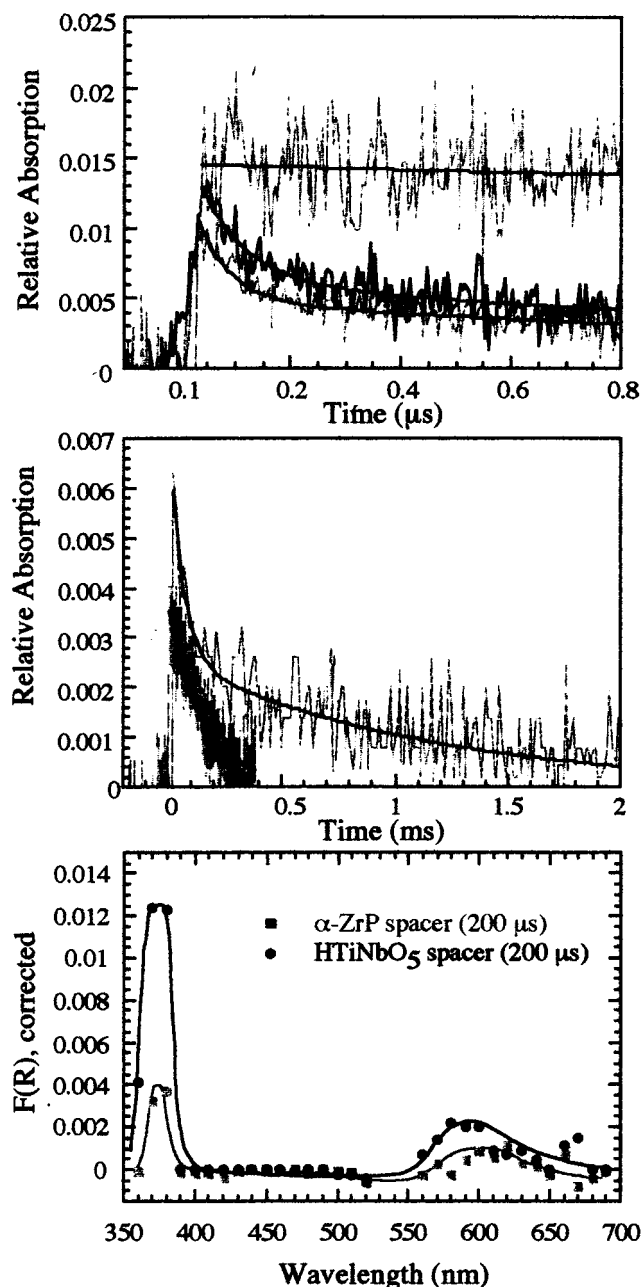
Figure 9. Top: 450 nm transient signals, showing the decay of the porphyrin triplet state, for the silica/amine/α-ZrP/PAH/α-ZrP/PAH/PdTSPP^{4-} "actinometer" (upper gray transient), silica/amine/α-ZrP/PVT-MV^{2+}/α-ZrP/PAH/PdTSPP^{4-} (middle black transient), and silica/amine/α-ZrP/PVT-MV^{2+}/HTiNbO$_5$/PAH/PdTSPP^{4-} (lower gray transient) samples. Middle: 600 nm transients, showing the decay of the reduced viologen charge separated state, for samples containing HTiNbO$_5$ (upper transient) and α-ZrP (lower transient) spacers between viologen and porphyrin layers. Bottom: Transient diffuse reflectance spectra taken 200 μs after 532 nm excitation, for samples containing HTiNbO$_5$ (upper) and α-ZrP (lower) spacers.

The sheet cannot mediate back electron transfer from these remote acceptors efficiently, because the viologen formal potential is positive of the flat-band potential. In quantitative terms, the additional static quenching component at 450 nm corresponds to 20% of the porphyrin excited states, and the long-lived charge-separated state to 18%. Effectively, HTiNbO$_5$ acts as the primary electron acceptor for a fraction of the ^{3}PdTSPP^{4-} electron donors, which are apparently properly positioned for electron injection into the sheets.

Conclusions

Layer-by-layer assembly provides a convenient route to fairly complex energy and electron transfer assemblies. Different chromophores and photoredox molecules are easily incorporated by derivatization of organic polyelectrolytes. Monomeric molecules with sufficiently high charge, such as PdTAPP^{4+} and PdTSPP^{4-}, can also be included in the polyelectrolyte adsorption process. The inorganic sheets α-ZrP and HTiNbO$_5$ serve to separate polycation layers, and act as 1 nm thick passive and active spacers, respectively, for electron-transfer reactions.

Energy transfer is a forgiving process, relative to electron transfer, because the back reaction is not an issue. A useful strategy is to mix the energy transfer components in a single polycation layer, or to make a cation/anion/cation sandwich between inorganic spacer sheets. The Coum-PAH, Fl-PAH, PdTAPP^{4+}, and Coum-PAH/PdTSPP^{4-}/Fl-PAH mixed layers are therefore more efficient light harvesting systems than stratified assemblies, such as Coum-PAH/α-ZrP/Fl-PAH/α-ZrP/PdTAPP^{4+}. However, separation of these light harvesting layers from the electron acceptor layer PVT-MV^{2+} is a useful design strategy, because the back electron-transfer reaction is inhibited by increasing separation distance. HTiNbO$_5$ actively mediates electron transfer for a fraction of the PdTSPP^{4-} excited states, and gives a very long-lived porphyrin-viologen charge separated transient. One of the interesting questions about the Coum-PAH/PdTSPP^{4-}/Fl-PAH/HTiNbO$_5$/PVT-MV^{2+} "pentad" system is why only about 15−20% of the excited-state molecules avail themselves of the mediated electron-transfer pathway. The sulfonate groups of the PdTSPP^{4-} sensitizer do not coordinate to the HTiNbO$_5$ sheets. However, other sensitizers, such as carboxylate- and phophonate-terminated Ru(bpy)$_3$$^{2+}$ derivatives, coordinate strongly and undergo fast electron-transfer reactions with HTiNbO$_5$.[19,31] In principle, structurally related porphyrin sensitizers might be used to increase the charge injection efficiency. These energy/electron transfer systems might also be coupled with an electron donor layer to increase the charge separation lifetime, and to provide an interface to an electrode or catalyst. These possibilities are currently under investigation.

Supporting Information Available: Descriptions are given of the procedure used to calculate Förster radii and energy transfer quantum yields, along with a listing of the FORTRAN program used. Spectral deconvolution and scattering correction factors are also described. This material is available free of charge via the Internet at http://pubs.acs.org.